Hindawi Publishing Corporation
International Journal of Photoenergy
Volume 2015, Article ID 630476, 12 pages
http://dx.doi.org/10.1155/2015/630476

Research Article

Synthesis, Analysis, and Testing of BiOBr-Bi_2WO_6 Photocatalytic Heterojunction Semiconductors

Xiangchao Meng and Zisheng Zhang

Department of Chemical and Biological Engineering, University of Ottawa, 161 Louis Pasteur, Ottawa, ON, Canada K1N 6N5

Correspondence should be addressed to Zisheng Zhang; zzhang@uottawa.ca

Received 24 January 2015; Revised 30 March 2015; Accepted 30 March 2015

Academic Editor: Leonardo Palmisano

In photocatalysis, the recombination of electron-hole pairs is generally regarded as one of its most serious drawbacks. The synthesis of various composites with heterojunction structures has increasingly shed light on preventing this recombination. In this work, a BiOBr-Bi_2WO_6 photocatalytic heterojunction semiconductor was synthesized by the facile hydrothermal method and applied in the photocatalytic degradation process. It was determined that both reaction time and temperature significantly affected the crystal structure and morphologies of the photocatalysts. BiOBr (50 at%)-Bi_2WO_6 composites were prepared under optimum synthesis conditions (120°C for 6 h) and by theoretically analyzing the DRS results, it was determined that they possessed the suitable band gap (2.61 eV) to be stimulated by visible-light irradiation. The photocatalytic activities of the as-prepared photocatalysts were evaluated by the degradation of *Rhodamine B (RhB)* under visible-light irradiation. The experimental conditions, including initial concentration, pH, and catalyst dosage, were explored and the photocatalysts in this system were proven stable enough to be reused for several runs. Moreover, the interpreted mechanism of the heterojunction enhancement effect proved that the synthesis of a heterojunction structure provided an effective method to decrease the recombination rate of the electron-hole pairs, thereby improving the photocatalytic activity.

1. Introduction

Photocatalysts are growing more prominent due to their essential role in most of today's environmental and energy-source problems. Since 1972, photocatalysis has been heavily researched and an increasing number of results have been published [1]. The involved fields mainly include hydrogen generation by water-splitting [2, 3] and the remediation of environmental problems related to industrial wastewater treatment [4], ground water purification [5, 6], disinfection [7, 8], and removal of air pollutants [9, 10]. Simultaneously, the defects of using photocatalysts were highlighted through their prosperous development specifically the low visible-light driven photocatalytic activities (commercially used photocatalysts-TiO_2 could only be activated by UV light) and the high recombination rates of the photogenerated electron-hole pairs.

Based on recent works, remediation trials aimed at overcoming the drawbacks mentioned above include modification of existing photocatalysts (e.g., metal deposition, doping, etc.) [11] and synthesis of novel photocatalysts with high-visible-light driven photocatalytic activities such as C_3N_4 [12], graphene [13], and bismuth composites (e.g., BiOX, X = F, Cl, Br, and I, Bi_2WO_6, etc.) [14, 15]. Bismuth composites have high visible-light photocatalytic activity due to their well-dispersed valence bands consisting of not only O 2p orbitals like in metal oxide semiconductors, but also Bi 6s orbitals. As a result, the composites have better separation of electron-hole pairs despite their narrow band gaps [16]. By adjusting the synthesizing conditions, a variety of morphologies of bismuth composites were prepared, such as nanoplate-like structures, microporous spheres, and hierarchical structures. This is because the structure of the photocatalyst, to some extent, influences their properties. For example, semiconductors with a 3D superstructure could have slightly narrower band gaps than plate-like semiconductors [15].

Heterojunction semiconductors are gradually emerging recently due to the enhancement effect on the photocatalytic

activity. Due to the high visible-light driven photocatalytic activity of bismuth composites and comparatively high recombination rate of the photogenerated electron-hole pairs, researchers focused on recombining two different bismuth composites to establish the heterojunction structure, in which the self-formed electric field could push the electrons and holes to opposite sides of heterojunction, effectively separating the charge carriers. Many heterojunction semiconductors with high photocatalytic degradation of pollutants have been reported that use either Bi_2WO_6 or BiOBr in the composite [17–22]. However, to the knowledge of the author, a BiOBr-Bi_2WO_6 heterojunction photocatalyst synthesized by the facile hydrothermal method has still not been reported. Theoretically, a BiOBr-Bi_2WO_6 composite has suitable band gap energy for simulation by visible-light irradiation and can be applied in the degradation of pollutants in dye water via generation of oxidative species such as hydroxyl radicals, superoxide radicals, and hydrogen peroxide.

This report presents the preparation of BiOBr-Bi_2WO_6 heterojunction semiconductors using the facile hydrothermal method. The crystal structures and morphologies of the as-prepared photocatalysts were observed by XRD and SEM techniques. DRS and classical Tauc formulation were applied to evaluate and calculate the band gap. The photodegradation of *Rhodamine B (RhB)* was used to measure the photocatalytic activity of the composites under visible-light irradiation (wavelength $\lambda > 410$ nm) in a slurry reactor. The influence of experimental conditions in synthesizing the samples and photocatalytic degradation process was explored and introduced. Finally the mechanism of the heterojunction enhancement effect was illustrated with the band structure.

2. Experimental

2.1. Synthesis of BiOBr-Bi_2WO_6 Composites. The facile hydrothermal method was used as the synthesis method to prepare the BiOBr-Bi_2WO_6 composites. All of the reagents were purchased from Sigma-Aldrich in their pure form. 2 g $Bi(NO_3)_3{\cdot}5H_2O$ was dissolved in 80 mL acetic acid and then dropwise added into the solution containing 0.45 g $Na_2WO_4{\cdot}2H_2O$ and 0.16 g KBr. Herein, the atomic ratio of BiOBr/Bi_2WO_6 was 1 : 1. The turbid liquid was then moved into 45 mL Teflon-lined stainless steel autoclaves (purchased from Parr Instrument Company) and magnetically stirred for 30 minutes under room temperature. Next, the autoclaves were heated in the oven at a designated temperature for a designated amount of time. In this work, the temperatures that were chosen are 90°C, 120°C, 150°C, 180°C, and 210°C, respectively. Meanwhile, the time of the heat preservation was 3 h, 6 h, 9 h, 12 h, and 15 h, respectively. After the autoclaves naturally cooled down to room temperature, the precipitate was separated by centrifugation (1500 rpm for 5 minutes) and finally dried in the oven (80°C for 12 h).

2.2. Characterization. The crystal structures were characterized by X-ray powder diffraction (XRD) with a Cu-Kα radiation Diffractometer at 40 kV and 44 mA recorded with 2θ scope ranging from 5 to 80°. As for the morphologies, field-emission scanning electron microscopy (FE-SEM) was used. The UV-Vis diffusion reflectance spectra of the photocatalysts were performed by a UV-Vis spectrophotometer (Thermo Evolution 300) equipped with an accessory to analyze powder samples.

2.3. Photocatalytic Reactor and Photocatalytic Activity Measurement. The photocatalytic reactor was a slurry batch photoreactor. The light source was a 300 W tungsten halide bulb (purchased from USHIO) with a cut-off filter (purchased from Kenko Zeta, transmittance > 90%) to filter out the irradiation with wavelengths below 410 nm so that the irradiation in this system is attributed only to visible light. The intensity of the irradiation was found to be approximately 4.7×10^{-3} Einstein$\cdot m^{-2}\cdot s^{-1}$ measured by a quantum meter (Biospherical QSL-2100; 400 nm < λ < 700 nm). The sufficiently high irradiation intensity aimed to prevent the dependence of the reaction rate on the generation of the electron-hole pairs, and the controlled factor of the photocatalytic activity was the mass transfer. A cooling jacket was applied outside the reactor, and the temperature of the degradation process was kept around (20 ± 2)°C. Meanwhile, the solid-liquid solution was stirred magnetically under 180 rpm to enhance the mass transfer.

Rhodamine B (RhB) was regarded as the polluting organic in the dye water. In each experiment, 200 mL of waste water (aqueous RhB solution) with a specific concentration was added into the 500 mL beaker, and a certain amount of the specific photocatalyst was mixed with the waste water under magnetic stirring for 30 min in the dark to attain the adsorption-desorption balance. The photocatalytic degradation was then performed for 2 hours in the presence of visible-light irradiation. About 1 mL of the suspension was taken out from the reactor every 10 min, and the supernatant solution was separated using the centrifuge and measured by UV-Vis spectrophotometer (Puxi, UV 1901). The peak absorbance for RhB was $\lambda = 554$ nm. The degradation efficiency of RhB was calculated using the following equation:

$$\omega_{\text{degradation efficiency}} = \frac{c_o - c_t}{c_o} \times 100\%, \quad (1)$$

where c_o is the initial concentration of RhB and c_t is the concentration of RhB at the specific testing time during the degradation.

To study the influencing factors of the degradation process, the initial concentration of RhB, pH of the dye water, and the dosage amount of the photocatalysts in the slurry system would be explored.

3. Results and Discussion

3.1. XRD Analysis. Two factors, the time of the heat preservation and the temperature in the synthesis process, were explored, and the crystal structures of the BiOBr-Bi_2WO_6 composites synthesized under different experimental conditions were measured by X-ray diffraction techniques, which were shown in Figures 1 and 2.

Firstly, the effect of holding time of the autoclaves in the oven was studied and shown in Figure 1. All of the XRD

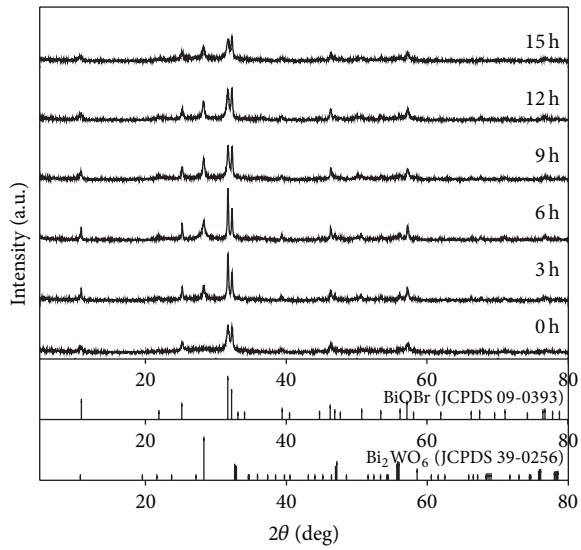

Figure 1: XRD pattern of the BiOBr-Bi_2WO_6 composites synthesized for various times at 120°C.

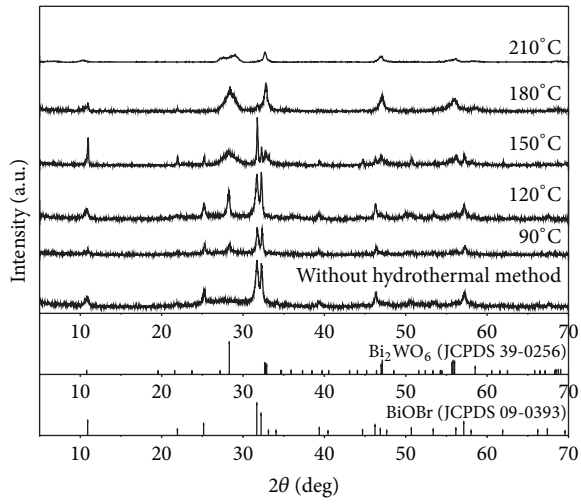

Figure 2: XRD pattern of BiOBr-Bi_2WO_6 composites synthesized by hydrothermal method for 6 h under various temperatures.

patterns synthesized under various holding times at 120°C showed that characteristic peaks were in good agreement with the tetragonal structure for BiOBr in the standard JCPDS card (09-0393) and the orthorhombic structure for Bi_2WO_6 in the standard JCPDS card (39-0256). With the holding time rising up to 6 h, the characteristic peaks became much sharper which signifies an increase in crystallinity. When the holding time exceeded 6 h, the outline and the intensity of the characteristic peaks were similar, which suggested that 6 h was enough for the synthesis of the BiOBr-Bi_2WO_6 composites just from the point of the crystal structure.

Secondly, the effect of the synthesis temperature of the autoclaves in the oven was studied, and the XRD pattern of the BiOBr-Bi_2WO_6 composites synthesized under various temperatures and holding 6 h was shown in Figure 2. It could be concluded that the composites before hydrothermal treatment singly consisted of tetragonal BiOBr, and with increasing temperature, the characteristic peaks of orthorhombic Bi_2WO_6 became more prominent such as the typical peak at $2\theta = 28.30^\circ$. When the temperature was over 120°C, the characteristic peaks of BiOBr became weaker and the characteristic peaks of Bi_2WO_6 became stronger. At 210°C, only some stunted characteristic peaks of Bi_2WO_6 were found. This phenomenon might be because temperatures higher than 120°C were in favor of the growth of Bi_2WO_6 and probably went against the growth of BiOBr [23]. The XRD results indicate that the crystal structures of BiOBr-Bi_2WO_6 composites could be selectively synthesized by adjusting the hydrothermal reaction holding time and temperature, and the well-crystallized BiOBr-Bi_2WO_6 composites could be synthesized with facile experimental conditions at 120°C for 6 h.

3.2. SEM Analysis. Field-emission scanning electron microscopy (FE-SEM) has been performed to analyze the morphologies of the as-prepared BiOBr-Bi_2WO_6 composites. The formation process of BiOBr-Bi_2WO_6 composites involved hydrothermal ripening, which is a common phenomenon in crystal growth process. Based on the images in Figure 3, it suggested that by increasing the reaction time from 3 h to 15 h (while keeping the temperature at 120°C) the structure changed from thin and irregularly shaped agglomerate nanoplates to flawless bigger microspheres. Specifically, when the reaction time was 6 h, the composites could be described as nanoplate-like BiOBr covered with flake-like Bi_2WO_6. When the reaction time exceeded 6 h, the size increase from about 1 μm (at 6 h) to about 8 μm (at 15 h) could be interpreted as the intrinsic anisotropic growth habit which could happen when the energy was high enough to overcome the reaction barriers (heated over 120°C in our system) [24]. The surface became much smoother due to the recrystallization process, which frequently took place during the hydrothermal synthesis of nanomaterials [25, 26]. The tighter the structure was, the lower the total energy of the system would be via minimal surface energy. SEM images of the photocatalysts synthesized under various temperatures for 6 h were shown in Figure 4. They were hierarchical microspheres with increasingly better-crystallized flake-like Bi_2WO_6 grown on the surface when the temperature increased from 90°C to 210°C. Combined with the results of XRD, it could be concluded that high temperatures selectively accelerated the formation of flake-like Bi_2WO_6. These results are highly consistent with the XRD results analyzed in the previous section and further prove that the structure of the BiOBr-Bi_2WO_6 composites could be controlled by adjusting the experimental conditions.

3.3. UV-Vis Diffuse Reflectance Spectrum (DRS) Analysis. Optical properties of the as-prepared photocatalysts were measured by their UV-Vis reflectance spectra. Figure 5 shows the reflectance spectra of samples including pure Bi_2WO_6, BiOBr (50 at%)-Bi_2WO_6 composite, pure BiOBr, and TiO_2

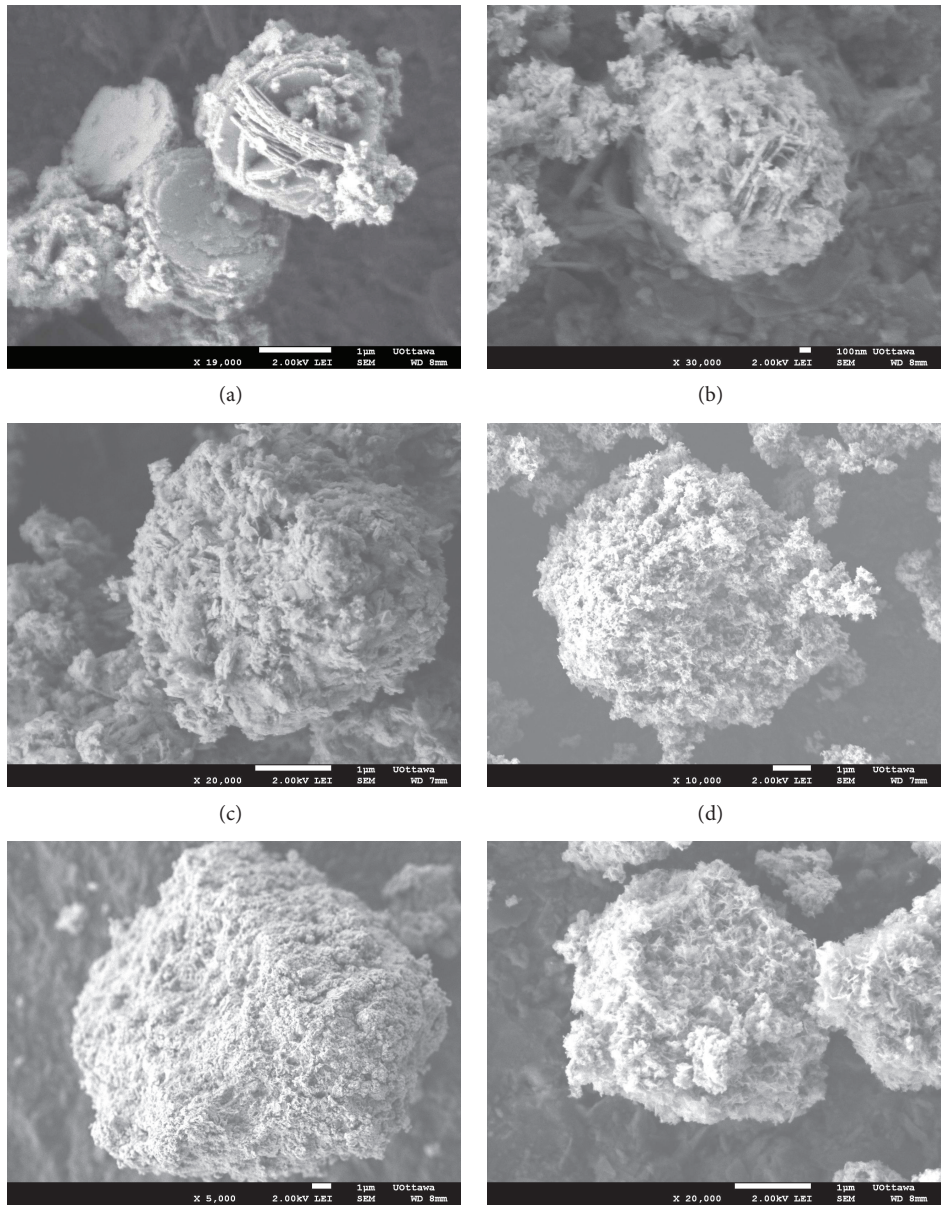

Figure 3: FE-SEM images of BiOBr-Bi_2WO_6 composites synthesized for (a) 3 h, (b) 6 h, (c) 9 h, (d) 12 h, and (e) 15 h under 120°C and that of (f) pure Bi_2WO_6.

(P25, anatase). All of these results exhibit a significant increase in absorbance at the wavelength of irradiation lower than some specific value. For the band gap transition, for example, the value for the BiOBr (50 at%)-Bi_2WO_6 composite was about 470 nm. Calculation of the band gap used the following classical Tauc equation for indirect semiconductors:

$$\alpha E_{\text{photon}} = K(E_{\text{photon}} - E_g)^{n/2}, \quad (2)$$

where $E_{\text{photon}} = h\nu$; α, K, E_g, n, h, and ν represent the absorption coefficient, constant for semiconductor (usually equal to 1), band gap energy, constant for semiconductor depending on the type of the band gap (for indirect transition: $n = 4$) [27–29], Planck constant, and irradiation frequency, respectively [30]. The band gap value (E_g) was extrapolated by plotting $(\alpha \times E_{\text{photon}})^{1/2}$ versus E_{photon} shown in Figure 5, and the band gaps were 3.10 eV, 2.80 eV, 2.61 eV, and 2.72 eV for TiO_2, pure Bi_2WO_6, BiOBr (50 at%)-Bi_2WO_6 composites, and pure BiOBr, respectively. They suggested that the bismuth composites are suitable for being activated by visible light and that TiO_2 could only be motivated by irradiation with wavelengths lower than 400 nm, that is, the ultraviolet region. Furthermore, a red-shift from 2.61 eV to 2.72 eV was observed when the BiOBr formed a heterojunction with Bi_2WO_6, which could be due to the notable effects of the shape and structure. SEM images of pure BiOBr, Bi_2WO_6, and the BiOBr (50 at%)-Bi_2WO_6 composites were shown in

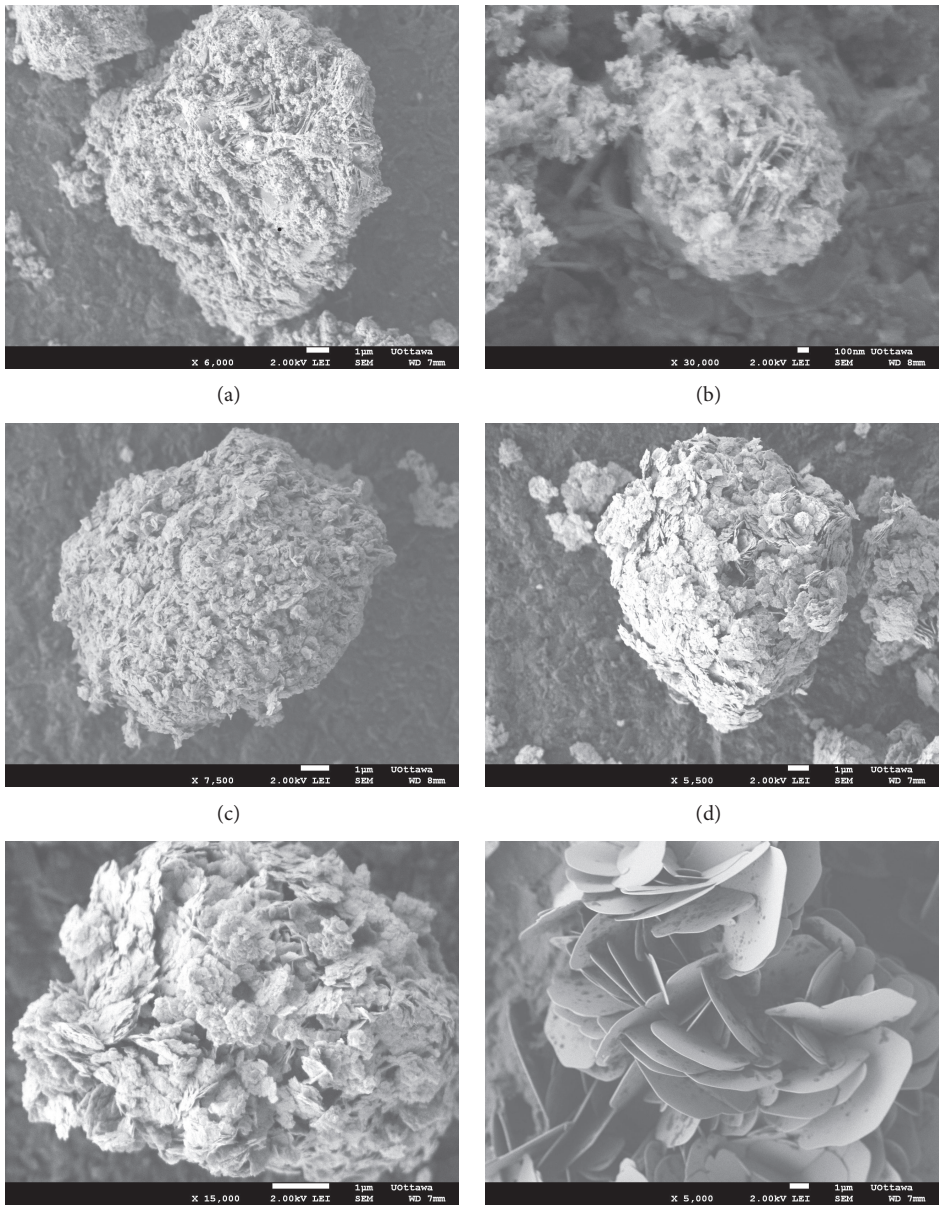

Figure 4: FE-SEM images of BiOBr-Bi_2WO_6 composites synthesized for 6 h under (a) 90°C, (b) 120°C, (c) 150°C, (d) 180°C, and (e) 210°C and that of (f) pure BiOBr.

Figures 3(f) and 4(f). The 3D superstructure of the BiOBr-Bi_2WO_6 heterojunction could decrease the band gap compared to the plate-like BiOBr; similar results appeared in [15]. In conclusion, synthesizing the novel photocatalysts (bismuth composites in this work) with suitable band gaps could theoretically widen the wavelength of the irradiation into the visible-light range.

3.4. Photocatalytic Performance in Degradation of RhB

3.4.1. Effect of Synthesizing Conditions. Photocatalytic activities of the as-prepared photocatalysts were evaluated by the degradation of RhB under visible-light illumination ($\lambda > 410$ nm). The degradation efficiencies for systems with photocatalysts synthesized at different reaction times and the same reaction temperature and for the same reaction time at different reaction temperatures were displayed in Figures 6 and 7, respectively. Calculated apparent reaction constants of each experiment were also summarized in Table 1. For reaction times, from 0 h to 6 h (0 h means photocatalysts without hydrothermal process and separated from the precursor directly) at 120°C, the degradation efficiency improved from 50% to 82% within the first 10 min. This phenomenon might correspond to the increasingly better-crystal heterojunction structure which could enhance the photocatalytic degradation by improving the separation of the electron-hole

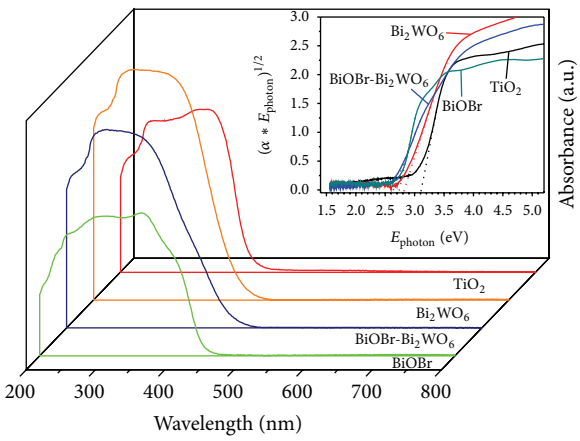

Figure 5: UV-Vis diffuse reflectance spectra (DRS) and $(\alpha * E_{photon})^{1/2} - E_{photon}$ curves of TiO_2 (anatase), pure Bi_2WO_6, and BiOBr-Bi_2WO_6 composites (pure Bi_2WO_6 and BiOBr were synthesized by the hydrothermal method).

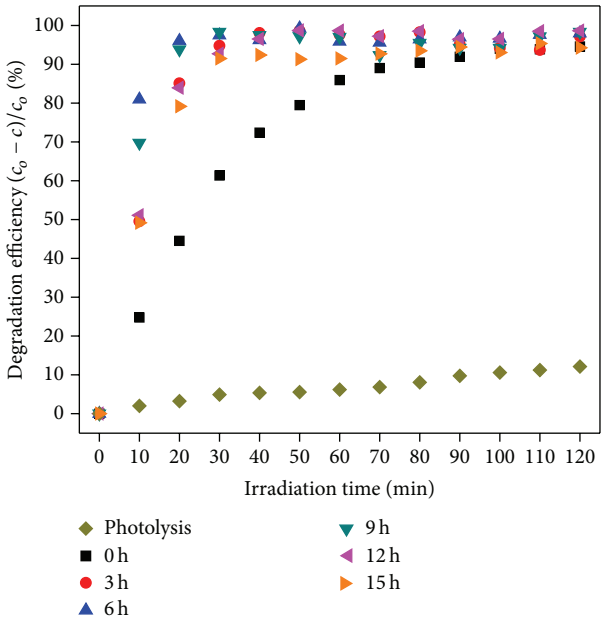

Figure 6: Photocatalytic degradation efficiency as a function of time by using the photocatalysts synthesized for various reaction times under 120°C (catalysts dosage: 1.0 g/L; temperature: (20 ± 2)°C; pH = 5; and initial concentration: 10 ppm).

pairs. From 10 min and onwards, deterioration in photocatalytic activity was probably caused by the decrease of surface defects that was introduced in Section 3.2. As for the photocatalytic activities of photocatalysts synthesized under different reaction temperature for the same reaction time, an optimum hydrothermal temperature existed at 120°C with approximately 100% degradation efficiency in just 20 min. This could be interpreted as temperatures higher or lower than 120°C hindered the establishment of the heterojunction.

Therefore, an optimum hydrothermal reaction time and temperature existed and were determined to be 6 h and

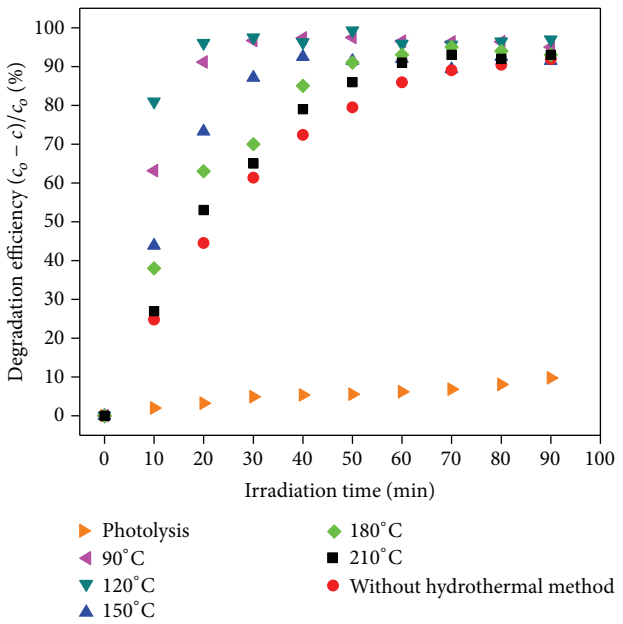

Figure 7: Photocatalytic degradation efficiency as a function of time by using the photocatalysts synthesized by hydrothermal method for 6 h under various hydrothermal reaction temperatures (catalysts dosage: 1.0 g/L; temperature: (20 ± 2)°C; pH = 5; and initial concentration: 10 ppm).

Table 1: Apparent kinetic constant of system with photocatalysts synthesized under different conditions.

Heat duration/h	Temperature/°C	Apparent rate constant/min^{-1}	R^2
0	120	0.03158	0.9952
3	120	0.1005	0.9832
6	120	0.1613	0.9995
9	120	0.1381	0.9961
12	120	0.08971	0.9899
15	120	0.08269	0.9940
6	90	0.1163	0.9916
6	150	0.06901	0.9994
6	180	0.03158	0.9952
6	210	0.01534	0.9952

120°C, respectively. These results are in good correspondence with the analysis of the crystal structure of the as-prepared photocatalysts as the structure significantly influenced the reactive performance.

3.4.2. Effect of Initial Concentration. Wastewater from different areas usually has varying concentrations of the pollutants. Therefore, the degradation of pollutants with varying initial concentrations is a significant parameter to analyze for photocatalysts. In this work, the initial concentration of RhB was varied from 5 ppm (mg/L) to 50 ppm (mg/L) with photocatalysts synthesized under the same conditions (120°C

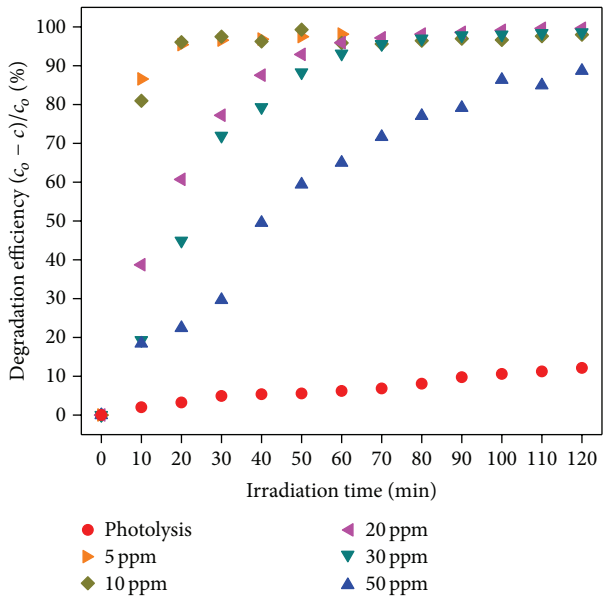

Figure 8: Photocatalytic degradation efficiency as a function of time in systems with various initial concentrations of RhB solution using BiOBr (50 at%)-Bi_2WO_6 composites synthesized for 6 h under 120°C (catalysts dosage: 1.0 g/L; temperature: (20 ± 2)°C; and pH = 5).

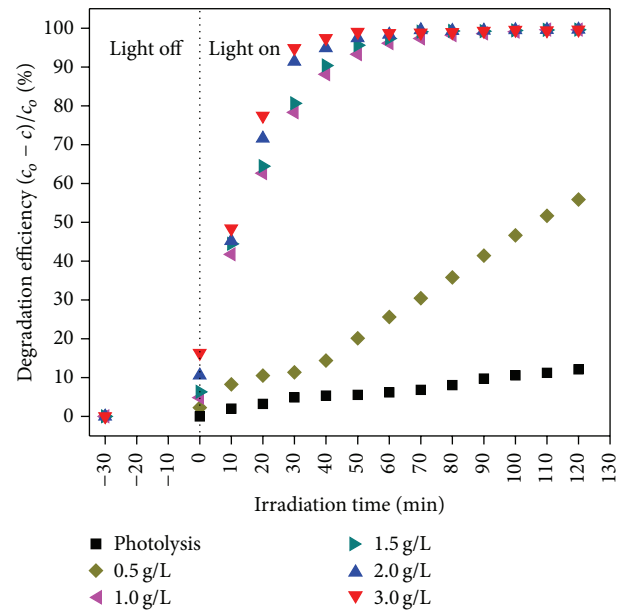

Figure 9: Photocatalytic degradation efficiency as a function of time in systems with various photocatalysts dosage by using BiOBr (50 at%)-Bi_2WO_6 composites synthesized for 6 h under 120°C (temperature: (20 ± 2)°C; pH = 5; and initial concentration: 20 ppm).

for 6 h) and the same experimental conditions such as photocatalyst dosage (1.0 g/L), pH (5), and reaction temperature (20 ± 2°C). The photocatalytic degradation efficiencies in these systems were shown in Figure 8. To investigate the influence of photolysis of RhB, the photolytic conversion at initial concentration of 10 ppm was measured and shown in Figure 8 and was found to be negligible. It could be observed that the RhB was completely removed in 20 min in the systems with an initial concentration of 5 ppm and 10 ppm, and by increasing the initial concentration of RhB from 20 ppm to 50 ppm, the degradation efficiency decreased from 60% to 22% in 20 min. These results could be ascribed to the degradation process which involves three individual processes: adsorption of RhB, reaction of RhB with oxidative species, and desorption of degraded products [31]. For a certain amount of the catalyst dosage (1.0 g/L), the adsorption and active sites were limited which resulted in increasing competition for RhB to be adsorbed and degraded with increasing concentration of the initial solution. Another reason is attributed to the reduction of the irradiation energy while passing through the solution. As expected when increasing the concentration of RhB, the color of the solution became much darker, which means much more irradiation energy would be lost before reaching the surface of the photocatalysts and it would correspondingly decrease the production efficiency of the electron-hole pairs. These two reasons finally resulted in the phenomenon that an increase of the initial solution concentration corresponds to a decrease in the degradation efficiency.

3.4.3. Effect of Photocatalysts Dosage. As a relatively expensive technique, it is significant to choose a suitable catalyst dosage for optimal degradation efficiencies. The dosage was varied from 0.5 g/L to 3.0 g/L (synthesized under 120°C for 6 h) and tested at the initial *RhB* concentration of 20 ppm and pH of 5, as shown in Figure 9. The photolytic effect of the irradiation was also measured in the system with initial concentration of 10 ppm and found to be negligible. As for the degradation efficiencies for different systems, it was surprisingly found an evident increase from about 10% to 40% when the catalyst dosage increased from 0.5 g/L to 1.0 g/L, and increasing the amount of the catalysts dosage up to 3.0 g/L then resulted in a tiny increase of the degradation efficiency in 30 min which was found as shown in Figure 10.

Meanwhile, before turning on the light, the adsorption-desorption ability in systems with different catalysts dosage was also investigated, and results suggested more of the photocatalysts in the system possessed much more active sites and were able to adsorb much more *RhB* before the photocatalytic process, which successfully explained the phenomenon that the photocatalytic activity could be enhanced by increasing the catalyst dosage. Beyond that, excessive amounts of the photocatalyst in the system would induce the increase of light scattering and decrease the irradiation penetration, thereby reducing the photocatalytic degradation efficiency [32, 33]. The integrated effects lead to the final results, which explained why intensive increase of the photocatalytic degradation efficiency has not occurred when the photocatalyst dosage was massively increased.

3.4.4. Effect of pH of the RhB Solution. The photodegradation of *RhB* with varying initial pH and fixed experimental conditions (initial concentration of 20 ppm, catalyst dosage of 1.0 g/L, and photocatalysts synthesized for 6 h under 120°C)

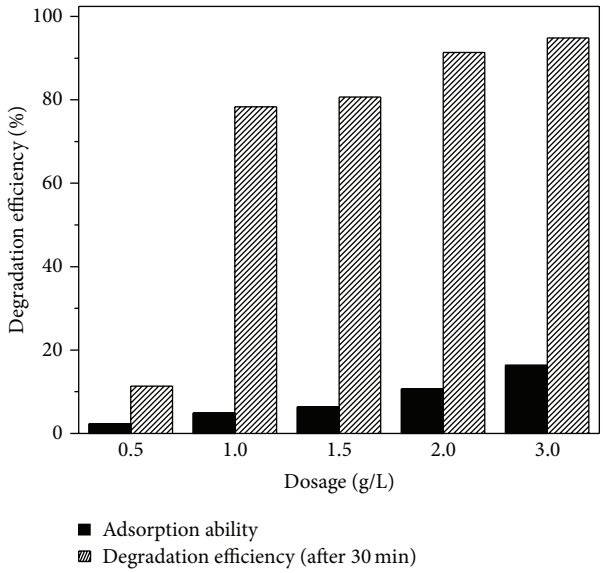

Figure 10: The adsorption abilities and photocatalytic degradation efficiency (in 30 min) in systems with various photocatalysts dosages using BiOBr (50 at%)-Bi_2WO_6 composites synthesized for 6 h under 120°C (temperature: (20 ± 2)°C; pH = 5; and initial concentration: 20 ppm).

was displayed by measuring the UV-Vis spectra as shown in Figure 11 (HCl and NaOH have been used to adjust the pH). It could be easily concluded from the results that different initial pH directly determined the mechanism of the degradation of *RhB*. Specifically, it could be seen that when the pH of the *RhB* solution was equal to 5, 7, and 9, these degradation processes have similar mechanisms. That is, the *RhB* was step-by-step degraded into *Rhodamine* by deethylation, observed by the blue-shift of the widely introduced characteristic peak from 554 nm (*Rhodamine B*) to 498 nm (*Rhodamine*) [31, 34, 35]. Meanwhile, with the increase of the pH from 5 to 9, the photocatalytic degradation efficiency decreased, which is attributed to the reduced adsorption of *RhB* with increasing pH while the high adsorption at relatively lower pH promoted the degradation rate [36]. When the pH reached 12, the *RhB* hardly was adsorbed on the surface of the photocatalysts, resulting in negligible degradation efficiency in 2 h. As for a pH of 2, it took longer time (about 2 h compared to 1 h for the system with initial pH equal to 7) for the blue-shift from 554 nm to 498 nm, which means it would be much more difficult for RhB to reach complete deethylation. This could be attributed to Bi_2WO_6 being unstable and transforming into H_2WO_4 and Bi_2O_3 in the acidic solution [36, 37]. The transformation of Bi_2WO_6 damages the BiOBr-Bi_2WO_6 heterojunction and eventually reduces the photocatalytic activity.

While the pH influenced the adsorption of the pollutants onto the photocatalysts, the redox species were also influenced at varying pH. It could be concluded that at lower pH, the positive holes play the significant role while at neutral or alkaline circumstances hydroxyl radials were regarded as the major oxidative species [38–40]. The final results integrated all of these effects introduced above and it is concluded that the pH range from 5 to 9 is suitable for the as-prepared photocatalysts, and lower pH is preferable in this range.

3.5. Reusability. To evaluate the reusability of the photocatalysts used in the system, consecutive photocatalytic processes for 4 runs have been measured and the results were displayed in Figure 12. Between each run, photocatalysts were separated from the slurry by centrifugation. The used photocatalysts were then mixed with fresh dye water. Results show that the degradation efficiencies of *RhB* decreased from 100% (complete degradation) to 85% in 2 h. This proves that the as-prepared photocatalysts could be reused with relatively high photocatalytic activity. The run-by-run decrease in performance may be due to the intermediate products of degraded *RhB,* which were not completely degraded, to remain adsorbed on the surface of the photocatalysts. This would reduce the sorption ability of the photocatalysts, resulting in the decrease of the degradation efficiencies. The structure of the photocatalysts after the degradation process for 4 runs was detected by XRD, which was shown in Figure 13. All of the characteristic peaks of tetragonal BiOBr and orthorhombic Bi_2WO_6 came out in the XRD patterns of photocatalysts before and after the degradation for 4 runs, which means the main structure of the BiOBr-Bi_2WO_6 heterojunction was not destroyed and was stable enough. However, each of the peaks in the upper XRD pattern has been widened and not as sharp as that of the under XRD pattern, and it suggests the crystallinity has been reduced to some extent that exactly corresponds to the pollutants or the intermediate products being adsorbed and remaining on the photocatalysts. In conclusion, the BiOBr-Bi_2WO_6 photocatalysts synthesized by the hydrothermal method possess the stable properties and could be reused multiple times, which is a prerequisite for photocatalyst applications in practice.

3.6. The Mechanism of Heterojunction Enhancement. The degradation efficiency of the photocatalyst synthesized by the hydrothermal method under 120°C for 6 h was compared to the efficiency of the photocatalyst synthesized by mechanically mixing pure BiOBr and Bi_2WO_6 by the similar hydrothermal method under the same experimental conditions, in which the fixed ratio of BiOBr and Bi_2WO_6 was equal to 1 : 1. The results were demonstrated in Figure 14. Specifically, the degradation efficiency improved from 20% for mechanical mixing to 55% for chemical synthesis. The heterojunction photocatalyst took about 50 min to completely remove *RhB*, while it took 120 min to obtain the same degradation results from mechanical mixing. The evident enhancement was probably attributed to the establishment of the BiOBr-Bi_2WO_6 heterojunction that has been introduced in other references [22, 41–43]. Similarly, the enhancement effect could simply be illustrated by the analysis of the band structure shown in Figure 15. When stimulated by light energy ($h\nu$), electrons jump from the valence band to the conduction band, leaving behind positive holes on the valence band. In the presence of an electric field, there exists a force to drive the electrons from the conduction band of

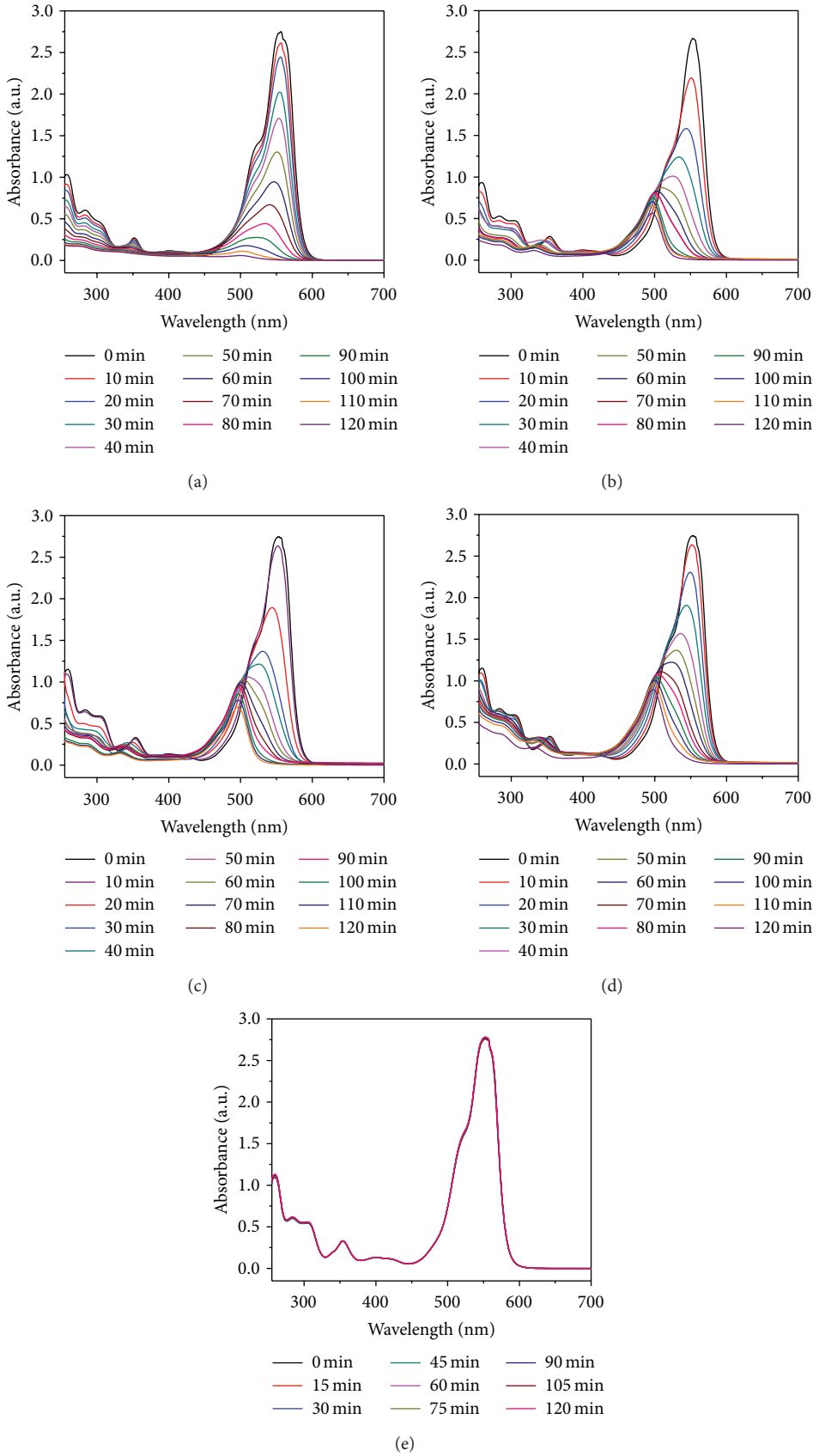

Figure 11: UV-Vis spectra of the samples taken during the degradation process and the *RhB* solutions with different initial pH: (a) pH = 2, (b) pH = 5, (c) pH = 7, (d) pH = 9, and (e) pH = 12 (photocatalysts: BiOBr (50 at%)-Bi_2WO_6 composites synthesized for 6 h under 120°C; catalysts dosage: 1.0 g/L; temperature: (20 ± 2)°C; and initial concentration: 20 ppm).

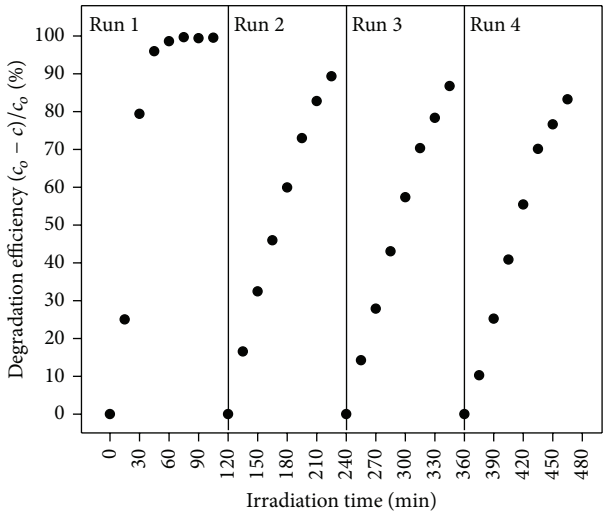

FIGURE 12: Photocatalytic degradation efficiency as a function of time in four runs (photocatalysts: BiOBr (50 at%)-Bi_2WO_6 composites synthesized for 6 h under 120°C; catalysts dosage: 1.0 g/L; temperature: (20 ± 2)°C; pH = 5; and initial concentration: 10 ppm).

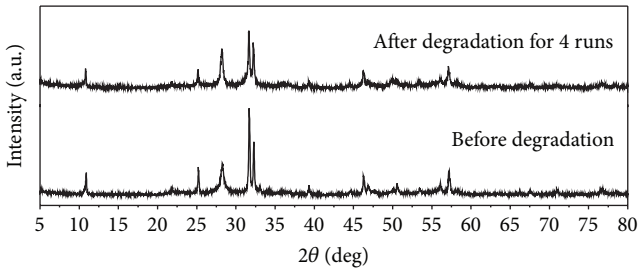

FIGURE 13: XRD pattern of photocatalysts (BiOBr (50 at%)-Bi_2WO_6 synthesized for 6 h under 120°C) before and after degradation process for 4 runs.

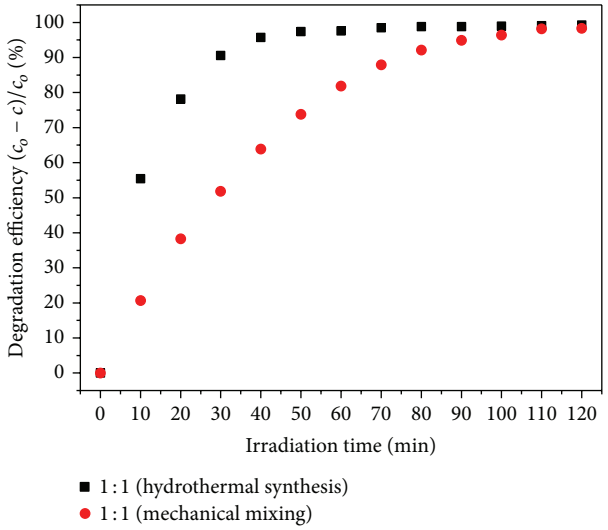

FIGURE 14: Degradation efficiency versus irradiation time by utilizing photocatalysts hydrothermally synthesized and mechanically mixed (ratio of BiOBr to Bi_2WO_6: 1 : 1; catalysts dosage: 0.5 g/L; temperature: (20 ± 2)°C; pH = 5; and initial concentration: 10 ppm).

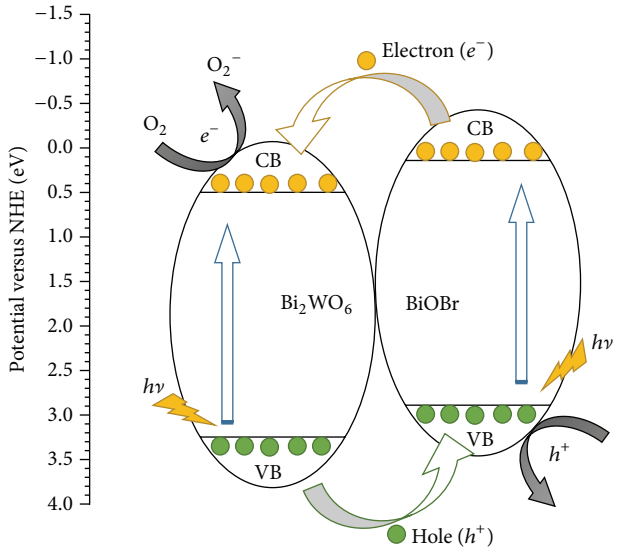

FIGURE 15: Band structure of the BiOBr-Bi_2WO_6 heterojunction (VB: valence band; CB: conduction band).

BiOBr to that of Bi_2WO_6, while holes oppositely move from the valence band of Bi_2WO_6 to that of BiOBr [27, 44]. This kind of movement effectively separates the electrons and holes so as to decrease the recombination rate of the electron-hole pairs. The accumulated electrons and holes could then individually react with adsorbed species such as oxygen or the organic pollutants.

4. Conclusions

In this work, novel BiOBr-Bi_2WO_6 heterojunction photocatalysts have been synthesized by the facile hydrothermal method. The optimal synthesis conditions, especially the hydrothermal reaction temperature (120°C) and holding time (6 h), have been explored and discussed on the basis of evaluating the sample's structure (XRD, SEM) and photocatalytic degradation efficiency. DRS results theoretically proved that BiOBr-Bi_2WO_6 composites have suitable band gaps to be stimulated by visible-light irradiation. Furthermore, the influence of experimental conditions in the photocatalytic degradation process, such as the initial concentration, amount of the photocatalyst dosage, and initial pH, has been studied and discussed. By recycling the photocatalysts, it proved that the BiOBr-Bi_2WO_6 composites were stable enough to be used in practice. Finally, the mechanism of the enhancement effect by establishing the heterojunction has been explained based on the band structure and further suggested it is an effective approach to separate the electron-hole pairs, enhancing the photocatalytic activity in the degradation of pollutants in dye water.

Conflict of Interests

The authors declare that there is no conflict of interests regarding the publication of this paper.

Acknowledgment

The authors hereby acknowledge the financial support of the work by the Natural Sciences and Engineering Research Council of Canada.

References

[1] A. Fujishima and K. Honda, "Electrochemical photolysis of water at a semiconductor electrode," *Nature*, vol. 238, no. 5358, pp. 37–38, 1972.

[2] M. Ni, M. K. H. Leung, D. Y. C. Leung, and K. Sumathy, "A review and recent developments in photocatalytic water-splitting using TiO_2 for hydrogen production," *Renewable and Sustainable Energy Reviews*, vol. 11, no. 3, pp. 401–425, 2007.

[3] X. Chen, S. Shen, L. Guo, and S. S. Mao, "Semiconductor-based photocatalytic hydrogen generation," *Chemical Reviews*, vol. 110, no. 11, pp. 6503–6570, 2010.

[4] C. Hachem, F. Bocquillon, O. Zahraa, and M. Bouchy, "Decolourization of textile industry wastewater by the photocatalytic degradation process," *Dyes and Pigments*, vol. 49, no. 2, pp. 117–125, 2001.

[5] J. C. Crittenden, Y. Zhang, D. W. Hand, D. L. Perram, and E. G. Marchand, "Solar detoxification of fuel-contaminated groundwater using fixed-bed photocatalysts," *Water Environment Research*, vol. 68, no. 3, pp. 270–278, 1996.

[6] M. S. Mehos and C. S. Turchi, "Field testing solar photocatalytic detoxification on TCE-contaminated groundwater," *Environmental Progress*, vol. 12, no. 3, pp. 194–199, 1993.

[7] J. C. Yu, W. Ho, H. Yip, K. W. Po, and J. Zhao, "Efficient visible-light-induced photocatalytic disinfection on sulfur-doped nanocrystalline titania," *Environmental Science and Technology*, vol. 39, no. 4, pp. 1175–1179, 2005.

[8] J. Lonnen, S. Kilvington, S. C. Kehoe, F. Al-Touati, and K. G. McGuigan, "Solar and photocatalytic disinfection of protozoan, fungal and bacterial microbes in drinking water," *Water Research*, vol. 39, no. 5, pp. 877–883, 2005.

[9] P. Pichat, J. Disdier, C. Hoang-Van, D. Mas, G. Goutailler, and C. Gaysse, "Purification/deodorization of indoor air and gaseous effluents by TiO_2 photocatalysis," *Catalysis Today*, vol. 63, no. 2–4, pp. 363–369, 2000.

[10] M. R. Hoffmann, S. T. Martin, W. Choi, and D. W. Bahnemann, "Environmental applications of semiconductor photocatalysis," *Chemical Reviews*, vol. 95, no. 1, pp. 69–96, 1995.

[11] S. G. Kumar and L. G. Devi, "Review on modified TiO_2 photocatalysis under UV/visible light: selected results and related mechanisms on interfacial charge carrier transfer dynamics," *Journal of Physical Chemistry A*, vol. 115, no. 46, pp. 13211–13241, 2011.

[12] S. C. Yan, Z. S. Li, and Z. G. Zou, "Photodegradation performance of g-C_3N_4 fabricated by directly heating melamine," *Langmuir*, vol. 25, no. 17, pp. 10397–10401, 2009.

[13] Q. Xiang, J. Yu, and M. Jaroniec, "Graphene-based semiconductor photocatalysts," *Chemical Society Reviews*, vol. 41, no. 2, pp. 782–796, 2012.

[14] X. Zhang, Z. Ai, F. Jia, and L. Zhang, "Generalized one-pot synthesis, characterization, and photocatalytic activity of hierarchical BiOX (X = Cl, Br, I) nanoplate microspheres," *The Journal of Physical Chemistry C*, vol. 112, no. 3, pp. 747–753, 2008.

[15] L. Zhang, W. Wang, L. Zhou, and H. Xu, "Bi_2WO_6 Nano- and microstructures: shape control and associated visible-light-driven photocatalytic activities," *Small*, vol. 3, no. 9, pp. 1618–1625, 2007.

[16] H. An, Y. Du, T. Wang, C. Wang, W. Hao, and J. Zhang, "Photocatalytic properties of BiOX (X = Cl, Br, and I)," *Rare Metals*, vol. 27, no. 3, pp. 243–250, 2008.

[17] J. Cao, X. Li, H. Lin, B. Xu, S. Chen, and Q. Guan, "Surface acid etching of $(BiO)_2CO_3$ to construct $(BiO)_2CO_3$/BiOX (X = Cl, Br, I) heterostructure for methyl orange removal under visible light," *Applied Surface Science*, vol. 266, pp. 294–299, 2013.

[18] G. Fu, G. Xu, S. Chen, L. Lei, and M. Zhang, "Ag_3PO_4/Bi_2WO_6 hierarchical heterostructures with enhanced visible light photocatalytic activity for the degradation of phenol," *Catalysis Communications*, vol. 40, pp. 120–124, 2013.

[19] J. Fu, Y. Tian, B. Chang, F. Xi, and X. Dong, "BiOBr-carbon nitride heterojunctions: synthesis, enhanced activity and photocatalytic mechanism," *Journal of Materials Chemistry*, vol. 22, no. 39, pp. 21159–21166, 2012.

[20] M. Hojamberdiev, K.-I. Katsumata, K. Morita, S. A. Bilmes, N. Matsushita, and K. Okada, "One-step hydrothermal synthesis and photocatalytic performance of $ZnWO_4/Bi_2WO_6$ composite photocatalysts for efficient degradation of acetaldehyde under UV light irradiation," *Applied Catalysis A: General*, vol. 457, pp. 12–20, 2013.

[21] L. Kong, Z. Jiang, T. Xiao, L. Lu, M. O. Jones, and P. P. Edwards, "Exceptional visible-light-driven photocatalytic activity over BiOBr-$ZnFe_2O_4$ heterojunctions," *Chemical Communications*, vol. 47, no. 19, pp. 5512–5514, 2011.

[22] H. Lin, H. Ye, X. Li, J. Cao, and S. Chen, "Facile anion-exchange synthesis of BiOI/BiOBr composite with enhanced photoelectrochemical and photocatalytic properties," *Ceramics International*, vol. 40, no. 7, pp. 9743–9750, 2014.

[23] A. Phuruangrat, P. Dumrongrojthanath, N. Ekthammathat, S. Thongtem, and T. Thongtem, "Hydrothermal synthesis, characterization, and visible light-driven photocatalytic properties of Bi_2WO_6 nanoplates," *Journal of Nanomaterials*, vol. 2014, Article ID 138561, 7 pages, 2014.

[24] M. Shang, W. Wang, and L. Zhang, "Preparation of BiOBr lamellar structure with high photocatalytic activity by CTAB as Br source and template," *Journal of Hazardous Materials*, vol. 167, no. 1–3, pp. 803–809, 2009.

[25] D. Ma, S. Huang, W. Chen, S. Hu, F. Shi, and K. Fan, "Self-assembled three-dimensional hierarchical umbilicate Bi_2WO_6 microspheres from nanoplates: controlled synthesis, photocatalytic activities, and wettability," *The Journal of Physical Chemistry C*, vol. 113, no. 11, pp. 4369–4374, 2009.

[26] G. Xi, K. Xiong, Q. Zhao, R. Zhang, H. Zhang, and Y. Qian, "Nucleation-dissolution-recrystallization: a new growth mechanism for t-selenium nanotubes," *Crystal Growth and Design*, vol. 6, no. 2, pp. 577–582, 2006.

[27] J. Xia, J. Di, S. Yin et al., "Solvothermal synthesis and enhanced visible-light photocatalytic decontamination of bisphenol A (BPA) by g-C_3N_4/BiOBr heterojunctions," *Materials Science in Semiconductor Processing*, vol. 24, no. 1, pp. 96–103, 2014.

[28] F. Amano, K. Nogami, and B. Ohtani, "Enhanced photocatalytic activity of bismuth-tungsten mixed oxides for oxidative decomposition of acetaldehyde under visible light irradiation," *Catalysis Communications*, vol. 20, pp. 12–16, 2012.

[29] H. Fu, S. Zhang, T. Xu, Y. Zhu, and J. Chen, "Photocatalytic degradation of RhB by fluorinated Bi_2WO_6 and distributions of

the intermediate products," *Environmental Science & Technology*, vol. 42, no. 6, pp. 2085–2091, 2008.

[30] L. Junqi, G. Zhanyun, W. Yu, and Z. Zhenfeng, "Three-dimensional TiO_2/Bi_2WO_6 hierarchical heterostructure with enhanced visible photocatalytic activity," *Micro & Nano Letters*, vol. 9, no. 2, pp. 65–68, 2014.

[31] T. Wu, G. Liu, J. Zhao, H. Hidaka, and N. Serpone, "Photoassisted degradation of dye pollutants. V. Self-photosensitized oxidative transformation of Rhodamine B under visible light irradiation in aqueous TiO_2 dispersions," *Journal of Physical Chemistry B*, vol. 102, no. 30, pp. 5845–5851, 1998.

[32] C. C. Wong and W. Chu, "The direct photolysis and photocatalytic degradation of alachlor at different TiO_2 and UV sources," *Chemosphere*, vol. 50, no. 8, pp. 981–987, 2003.

[33] M. A. Behnajady, B. Alizade, and N. Modirshahla, "Synthesis of Mg-doped TiO_2 nanoparticles under different conditions and its photocatalytic activity," *Photochemistry and Photobiology*, vol. 87, no. 6, pp. 1308–1314, 2011.

[34] T. Watanabe, T. Takizawa, and K. Honda, "Photocatalysis through excitation of adsorbates. 1. Highly efficient N-deethylation of rhodamine B adsorbed to cadmium sulfide," *The Journal of Physical Chemistry*, vol. 81, no. 19, pp. 1845–1851, 1977.

[35] F. Chen, J. Zhao, and H. Hidaka, "Highly selective deethylation of Rhodamine B: adsorption and photooxidation pathways of the dye on the TiO_2/SiO_2 composite photocatalyst," *International Journal of Photoenergy*, vol. 5, no. 4, pp. 209–217, 2003.

[36] H. Fu, C. Pan, W. Yao, and Y. Zhu, "Visible-light-induced degradation of rhodamine B by nanosized Bi_2WO_6," *The Journal of Physical Chemistry B*, vol. 109, no. 47, pp. 22432–22439, 2005.

[37] Y. Li, J. Liu, and X. Huang, "Synthesis and visible-light photocatalytic property of Bi_2WO_6 hierarchical octahedron-like structures," *Nanoscale Research Letters*, vol. 3, no. 10, pp. 365–371, 2008.

[38] C. Guillard, H. Lachheb, A. Houas, M. Ksibi, E. Elaloui, and J.-M. Herrmann, "Influence of chemical structure of dyes, of pH and of inorganic salts on their photocatalytic degradation by TiO_2 comparison of the efficiency of powder and supported TiO_2," *Journal of Photochemistry and Photobiology A: Chemistry*, vol. 158, no. 1, pp. 27–36, 2003.

[39] I. Poulios and I. Tsachpinis, "Photodegradation of the textile dye Reactive Black 5 in the presence of semiconducting oxides," *Journal of Chemical Technology & Biotechnology*, vol. 74, no. 4, pp. 349–357, 1999.

[40] W. Z. Tang, Z. Zhang, H. An, M. O. Quintana, and D. F. Torres, "TiO_2/UV photodegradation of azo dyes in aqueous solutions," *Environmental Technology*, vol. 18, no. 1, pp. 1–12, 1997.

[41] S. Obregón and G. Colón, "Erbium doped TiO_2-Bi_2WO_6 heterostructure with improved photocatalytic activity under sun-like irradiation," *Applied Catalysis B: Environmental*, vol. 140-141, pp. 299–305, 2013.

[42] Y. Peng, M. Yan, Q.-G. Chen, C.-M. Fan, H.-Y. Zhou, and A.-W. Xu, "Novel one-dimensional Bi_2O_3-Bi_2WO_6 p-n hierarchical heterojunction with enhanced photocatalytic activity," *Journal of Materials Chemistry A*, vol. 2, no. 22, pp. 8517–8524, 2014.

[43] M. Shang, W. Wang, L. Zhang, S. Sun, L. Wang, and L. Zhou, "3D Bi_2WO_6/TiO_2 hierarchical heterostructure: controllable synthesis and enhanced visible photocatalytic degradation performances," *The Journal of Physical Chemistry C*, vol. 113, no. 33, pp. 14727–14731, 2009.

[44] J. Xia, J. Di, S. Yin et al., "Facile fabrication of the visible-light-driven Bi_2WO_6/BiOBr composite with enhanced photocatalytic activity," *RSC Advances*, vol. 4, no. 1, pp. 82–90, 2014.